58445

MICROSTRUCTURAL AND MECHANICAL PROPERTIES OF NANOSTRUCTURED Ti-Si-N COATINGS*

W. J. Meng, X. D. Zhang, B. Shi, J. C. Jiang and R. C. Tittsworth*
Mechanical Engr. Dept.
*Center for Advanced Microstructures and Devices
Louisiana State Univ.
Baton Rouge, LA

L. E. Rehn and P. M. Baldo
Materials Science Division
Argonne National Laboratory
Argonne, IL 60439

March 2002

Distribution:
1.-2. PRS (203)
3. Editorial Office
4-5. Authors
6. R. C. Birtcher
7. File

Submitted to Int. Conf. on Metallurgical Coatings and Thin Films, San Diego, CA on April 22-26, 2002.

*Work supported by Louisiana Board of Regents through contracts LEQSF(2000-03)-RD-B-03 and LEQSF(2001-04)-RD-A-07, the NSF through grant #DMI-0124441 and by the U.S. Department of Energy, Office of Science under Contract W-31-109-ENG-38.

Microstructure and Mechanical Properties of Nanostructured Ti-Si-N Coatings

W. J. Meng, X. D. Zhang, B. Shi, J. C. Jiang
Mechanical Engineering Department, Louisiana State University, Baton Rouge, LA 70803

L. E. Rehn, P. M. Baldo
Materials Science Division, Argonne National Laboratory, Argonne, ILL 60439

R. C. Tittsworth
Center for Advanced Microstructures and Devices, Louisiana State University, Baton Rouge, LA 70803

ABSTRACT:

We have synthesized a series of Ti-Si-N coatings with 0 to 20 at. % Si by high-density plasma-assisted vapor-phase deposition. Composition, structure, and atomic short-range order were characterized by Rutherford Backscattering Spectrometry (RBS), Transmission Electron Microscopy (TEM), Θ–2Θ X-ray Diffraction (XRD), and X-ray Absorption Near Edge Structure (XANES) spectroscopy. The mechanical properties of these coatings were characterized by instrumented nanoindentation, and compared to those of B1-TiN. Our experiments show that the present series of Ti-Si-N coatings are nanocomposites, consisting of a nm-scale mixture of crystalline titanium nitride (TiN) and amorphous silicon nitride (a-Si:N). The mechanical response of the present series of Ti-Si-N coatings was found to be essentially independent of the Si composition, and similar to that of B1-TiN.

INTRODUCTION

Ceramic coatings have been utilized in surface engineering applications for over two decades [1]. Recent investigations have concentrated on nanostructured ceramics for improving the performance of macro-scale [2] and micro-scale [3] mechanical systems. Mixing two or more phases on the nm length scale has been reported to lead to significant increases in coating hardness [4] and toughness [5] beyond the intrinsic properties of the constituent phases. In spite of these activities, a fundamental understanding of deformation and fracture mechanisms in nanostructured ceramics is currently lacking. Conflicting experimental results have appeared in the literature. In the Ti-containing hydrocarbon (Ti-C:H) coating system, both the presence [6] and absence [7] of a pronounced hardness peak around 40 at. % Ti have been reported. In the Ti-Si-N coating system, coating hardnesses ranging from 40 to 80 GPa have been reported in the composition range of 2 – 20 at. % Si [8], significantly exceeding the hardness of crystalline B1-TiN [9] [10]. It was proposed that these extraordinary mechanical properties could be understood by applying conventional fracture mechanics to dimensions relevant to the two-phase nanocomposite microstructure of Ti-Si-N [11]. Detailed characterization of the microstructure of Ti-Si-N coatings and how the coating microstructure influences mechanical response is therefore critical for understanding the deformation and fracture mechanisms in nanostructured ceramics.

This paper describes the characterization of the microstructure and mechanical response of a series of Ti-Si-N coatings with the Si composition in the range from 0 to 20 at. %. Coating composition was measured by Rutherford Backscattering Spectrometry (RBS). Structural characterization was carried out with θ-2θ X-ray Diffraction (XRD) and Transmission Electron Microscopy (TEM). Atomic short-range order surrounding Ti and Si atoms was probed by X-ray Absorption Near Edge Structure (XANES) spectroscopy. Coating mechanical response was measured by instrumented nanoindentation. Results of the present study show that this series of Ti-Si-N coatings consists of a nm-scale mixture of crystalline titanium nitride (TiN) and amorphous silicon nitride (a-Si:N). The mechanical response of the present series of Ti-Si-N coatings was found to be similar to that of B1-TiN, and essentially independent of the Si composition.

EXPERIMENTAL

Deposition of Ti-Si-N coatings was carried out in a hybrid chemical vapor deposition (CVD)/physical vapor deposition (PVD) tool, with a base pressure ~ 4×10^{-7} Pa. This tool combines a 13.56 MHz inductively coupled plasma (ICP) with four balanced magnetron sputter guns, and

enables independent control of ion energy and flux [12]. During Ti-Si-N deposition, one pair of facing magnetrons was fitted with two Ti (99.99%) targets and operated at the same cathode current. The other pair was fitted with two Si (99.99%) targets and operated at the same cathode current. Two-inch diameter Si(100) wafers were used as substrates. Prior to coating deposition, the Si substrate surface was etched in a pure Ar ICP, with a total ICP input power of 1000W and a dc substrate bias of –100 V. Deposition of a Ti-Si-N layer in an Ar(99.999%)/N_2(99.999%) mixture followed immediately after substrate etching. During deposition, the substrates were rotated continuously at the center of the deposition zone, and subjected to a constant bias of –50 V. Ar and N_2 gas input flow rates were fixed at 10.0/1.1 and the total pressure was kept at ~ 0.24 Pa during all depositions. By fixing the Ti cathode current at 1.0 A and raising the Si cathode current, a series of Ti-Si-N coatings were deposited with increasing Si composition. No intentional substrate cooling or heating was applied during deposition. Separate substrate temperature measurements made by attaching type K thermocouples to a sacrificial substrate showed that the substrate temperature was ~ 260 ^{o}C during deposition, due to heating by the high-density plasma. A similarly prepared silicon nitride/Si(100) specimen and a heteroepitaxial B1-TiN/Si(111) specimen grown at 800 ^{o}C [9] were also synthesized to compare with the Ti-Si-N coatings.

Coating composition was measured by RBS using a 1.6 MeV He^+ ion beam and a surface barrier detector at 135 degrees to the beam direction. The specimens were tilted toward the detector, 10 degrees off the normal to the beam. XRD in the θ-2θ geometry was carried out on a Rigaku Miniflex diffractometer using Cu Kα radiation. TEM examinations were performed in a JEOL JEM2010 microscope operated at 200 kV. Cross-sectional TEM specimens were prepared by gluing two coated Si wafer slices face-to-face, polishing to a thickness of 80-100 μm, dimple grinding to a thickness of < 20 μm, followed by 4 kV Ar^+ ion milling from both sides until perforation. Plan-view TEM specimens were prepared by polishing the Si substrate side to a thickness of ~ 60 μm, dimple grinding to a thickness of < 20 μm, 4 kV Ar^+ ion milling from the Si substrate side until perforation, followed by a brief ion milling from both sides prior to examination to remove possible contamination due to re-deposition. A Gatan Model 656 Dimple Grinder and a Gatan Model 691 Precision Ion Polishing System were used. Camera constant calibration for selected area electron diffraction patterns (SADPs) was accomplished by examining zone-axis single-crystal diffraction patterns from the Si substrate at the same camera length setting.

XANES spectroscopy was performed at the Double Crystal Monochromator (DCM) beamline at the Louisiana State University Center for Advanced Microstructures and Devices (LSU CAMD) synchrotron facility. Ti K-edge and the Si K-edge XANES spectra were collected using the total electron yield (TEY) technique at ambient temperature [13]. The total electron current from the specimen was measured with a Lytle detector biased at +45 V in a chamber with flowing He gas [14]. The incident photon beam intensity was monitored with a He-filled ionization chamber. Photon energy selection was provided by a Ge(220) and an InSb(111) double crystal monochromator at the Ti K-edge and Si K-edge, respectively. XANES measurements consisted of step scans in different energy regions relative to the edge position, ~ 4970 eV and ~ 1840 eV for Ti and Si K-edges, respectively. A typical Si K-edge scan consisted of 0.55, 0.15, and 0.35 eV steps in the regions 1810 – 1835, 1835 – 1855, and 1855 – 1900 eV, respectively. A typical Ti K-edge scan consisted of 1.05, 0.35, and 0.65 eV steps in the regions 4930 – 4955, 4955 – 5010, and 5010 – 5100 eV, respectively. An integration time of 1 sec per step was used. Up to six spectra were acquired consecutively from each specimen and averaged. Spectra from the Ti-Si-N specimens were compared to that of the silicon nitride/Si(100) specimen at the Si K-edge and that of the TiN/Si(111) specimen at the Ti K-edge.

Instrumented nanoindentation with a Berkovich diamond indenter was carried out using a Hysitron Triboscope interfaced to a Digital Instrument Dimension 3100 Atomic Force Microscope (AFM). The instrument load frame compliance and indenter tip area function were calibrated with a vendor supplied fused silica specimen in the load range of 13000 – 400 μN. This range of indenter loads corresponds to a contact depth on fused silica of 20 nm < h_c < 220 nm. Indentations on the Ti-Si-N specimens were carried out in the load range of 11 – 1 mN. The Oliver/Pharr analysis procedure was followed to extract modulus and hardness from the experimental load vs. displacement curves [15]. Values of the indentation modulus, $E_{ind} = E/(1-\nu^2)$, where E and ν are respectively the Young's modulus and Poisson's ratio, and the hardness, H, measured at 1 mN load, corresponding to h_c < 25 nm, were taken as being representative of the Ti-Si-N coatings. Four to eight indentations were performed at the same load and the results averaged. Surface morphology of the Ti-Si-N coatings was examined by contact mode AFM using the Berkovich diamond indenter as the scanning tip.

RESULTS and DISCUSSION

Figure 1 shows a contact AFM image of the as-deposited surface of a Ti-Si-N coating with a Si composition of 19.2 at. %. The surface morphology shown is representative of the entire series of Ti-Si-N coatings. Additional AFM imaging showed that the average roughness (R_a) of the as-deposited coatings was ~ 2 nm, independent of the Si composition.

Figure 2(a) shows RBS spectra from four Ti-Si-N/Si(100) specimens deposited at Si cathode currents of 0.30, 0.22, 0.16, and 0.10 A, respectively. Simulations assuming uniform composition as a function of depth within the Ti-Si-N layer are also shown and agree well with the measured spectra [16]. Oxygen and carbon impurity levels are below the detection limit of ~ 1 at. %, while the Ar level within the Ti-Si-N layer ranges from 1 to 2.5 at. %, typical of coatings deposited in Ar containing plasmas. The N composition increases approximately linearly from 50.0 to 56.5 at. % as the Si cathode current increases from 0.10 to 0.30 A. Figure 2(b) shows Ti and Si compositions of the Ti-Si-N coatings as a function of the Si cathode current. The Si composition increases monotonically from < 1 to ~ 20 at. % with increasing Si cathode current. Through fitting the RBS spectrum of the silicon nitride/Si(100) specimen, its composition was determined to be 54.7 at. % N, 40.9 at. % Si, 4 at. % Ar, and 0.4 at. % Ti. The N to Si ratio of this specimen is 1.337, almost identical to that for Si_3N_4. The density of this coating is ~ 3.3 g/cm^3 based on the RBS measurement and a cross-sectional TEM measurement of coating thickness. Thicknesses determined by cross-sectional TEM of the present series of Ti-Si-N coatings ranged from 110 to 130 nm.

Figure 3(a) shows a cross-sectional TEM micrograph of a Ti-Si-N coating with 7.0 at. % Si, which clearly shows the presence of crystalline columns, 5 – 10 nm in width and over 10 nm in height in the growth direction. A cross-sectional TEM micrograph of the silicon nitride/Si(100) specimen, Figure 3(b), shows that the specimen is of an uniform amorphous structure, i.e., it is a-Si:N. There is no evidence of any crystalline precipitates in Figure 3(b), suggesting that the 0.4 at. % Ti is dissolved uniformly within the a-Si:N matrix. Cross-sectional TEM examination of other Ti-Si-N coatings consistently shows the nanocrystalline columnar structure. Figures 4(a), 4(b), and 4(c) show cross-sectional SADPs from three Ti-Si-N coatings with Si compositions of 0.3, 7.0, and 19.2 at. %, respectively. The SADPs were taken from regions which included the Si substrate. All crystalline diffraction signatures from the Ti-Si-N coatings can be indexed to a cubic structure with lattice parameters of 4.22 - 4.23 Å, i.e., close to the 4.24 Å of bulk B1-TiN [17]. The SADPs show that the only crystalline phase present within this series of Ti-Si-N coatings is consistent with B1-

TiN. The existence of texture is also evident, with TiN(200) in parallel with Si(200), indicating a dominant TiN<100> texture in the growth direction, independent of the Si composition. Figure 4(d) shows a plan-view SADP from the Ti-Si-N coating with 19.2 at. % Si, showing in-plane random orientation of TiN. Figure 5(a) shows a θ-2θ XRD pattern of a Ti-Si-N coating with 19.2 at. % Si. Consistent with electron diffraction results shown in Figure 4, the only crystalline reflection originating from the coating is that of TiN(200). Additional XRD results show strong TiN<100> texture in the growth direction for the entire series of Ti-Si-N coatings. Assuming that the width of the TiN(200) reflection arises solely from grain-size broadening, an estimated TiN column height in the growth direction is obtained as a function of the Si composition through the Scherrer formula. Figure 5(b) shows that the estimated column heights are less than 40 nm. Figures 6(a) and 6(b) show two cross-sectional high-resolution TEM images of two Ti-Si-N coatings with Si compositions of 0.3 and 19.2 at. %, respectively. The high-resolution images clearly show that the coatings consist of columnar-like nanocrystalline grains. At 0.3 at. % Si, individual TiN grains are 5 - 10 nm in width and > 10 nm in height. They appear to be dislocation free, and most grain boundaries appear to be atomically sharp. At 19.3 at. % Si, columnar-like nanocrystalline TiN grains are 2 – 5 nm in width and > 10 nm in height. Amorphous regions now separate these nanocrystalline columns. The nanocrystalline/amorphous interfaces appear to be atomically sharp. The height of individual TiN nanocrystalline columns in the growth direction appears consistent with that estimated from XRD.

XANES spectra of a number of Ti-Si-N coatings are shown in Figure 7. Pre-edge backgrounds have been fitted to a linear function and removed. All spectra have been normalized to unit edge jump. Figure 7(a) shows normalized Ti K-edge XANES spectra of a number of Ti-Si-N coatings. The Ti K-edge spectrum of the B1-TiN/Si(111) specimen is shown in Figure 7(a) for comparison. At all Si compositions, the Ti K-edge XANES oscillations exhibit a one-to-one correspondence with those of the B1-TiN specimen, indicating that the short-range order surrounding the Ti atoms within the Ti-Si-N coatings is predominantly B1-TiN like. The normalized Si K-edge XANES spectra of the same set of Ti-Si-N coatings are shown in Figure 7(b). The Si K-edge spectrum of the a-Si:N/Si(100) specimen is also shown for comparison. Figure 7(b) shows that, at all Si compositions, the overall spectral shape of the Ti-Si-N coating spectrum is similar to that of a-Si:N. The a-Si:N spectral shape is relatively featureless, with a pronounced white line peaking around 1846 eV and one additional broad peak around 1860 eV, consistent with an

amorphous structure. The Ti-Si-N coating spectra exhibit appreciable differences in the edge region as compared to that of the a-Si:N specimen. The transition threshold begins at ~ 1838 eV for the Ti-Si-N coatings, as compared to ~ 1841 eV for the a-Si:N specimen. The difference becomes more pronounced as the overall Si composition decreases. As the Si composition decreases, the peak of the white line also shifts from 1845.3 to 1846.6 eV. Figure 7(c) shows two Si K-edge XANES spectra taken from an identical Ti-Si-N specimen with 7.0 at. % Si. The two spectra were taken with the InSb(111) DCM fully tuned and 50% detuned, respectively [18]. The close agreement between the two spectra indicates that possible distortion of the Si K-edge spectral features due to the presence of higher order harmonics is insignificant in the present set of data.

The overall spectral similarity of the Si K-edge XANES from the Ti-Si-N coatings to that from a-Si:N suggests that Si atoms incorporate into the Ti-Si-N coatings in an a-Si:N-like environment. This spectral similarity supports the lack of significant Si incorporation into the B1-TiN phase. It is, however, believed that the spectral differences in the edge and white-line regions between the Ti-Si-N coatings and the a-Si:N specimen are suggestive of some Ti atoms being present within the first few coordination shells of Si, in addition to Si and N atoms. Without Si substitution into B1-TiN, proximity of Si and Ti atoms can arise by either Ti atom dissolution within the a-Si:N phase or preferential Ti – Si bonding across TiN/a-Si:N interfaces. In the latter case, with decreasing Si composition, the fraction of such bonds is expected to increase because the surface to volume ratio of the a-Si:N phase increases. This is consistent with the observed gradual changes seen in the Si K-edge XANES spectra as the overall Si composition decreases. The dissolution limit of Ti atoms within the a-Si:N phase has not been determined, although the present experiments show that it is greater than 0.4 at. % Ti. For the present series of Ti-Si-N coatings, the Ti and Si K-edge XANES spectra indicate that there is no significant Si incorporation into the B1-TiN phase, that short-range-order surrounding Ti and Si atoms is, respectively, B1-TiN and a-Si:N like. The latter finding corroborates the TEM evidence. Taken together, the TEM images and XANES spectroscopy data demonstrate that this series of Ti-Si-N coatings consists of a nm-scale mixture of a B1-TiN phase and an a-Si:N phase, i.e., they are TiN/a-Si:N nanocomposites.

Figures 8(a) and 8(b) show load vs. displacement curves for two Ti-Si-N coatings with 7.0 and 11.9 at. % Si, respectively. A peak load of 1 mN was used in both cases. In both figures, an identical set of load vs. displacement curves for the B1-TiN specimen are also shown for comparison. For both Ti-Si-N specimens, the loading curve and the depth at peak load are

essentially identical to those for B1-TiN, while the initial unloading stiffness is less than that for B1-TiN. The lower initial unloading stiffness indicates that the Ti-Si-N coatings possess a lower elastic modulus (E_{ind}) than does B1-TiN. The hardness value can be defined as the peak load divided by either the indenter contact area under load or the remnant area after the load is completely removed [15]. Independent of how the hardness value is calculated, the complete load vs. displacement data show that the present Ti-Si-N coatings offer essentially the same resistance to indenter penetration as B1-TiN. Indentations performed on Ti-Si-N coatings at other Si compositions yielded similar results, as shown in Figure 8(c), which indicates no significant variation of E_{ind} and H as a function of the Si composition. Over the Si composition range of 0 – 20 at. %, hardness values of the present series of Ti-Si-N coatings determined from the Oliver/Pharr procedure do not significantly exceed 24 GPa. As expected, the measured elastic modulus and hardness of a-Si:N are lower than those for B1-TiN.

Percolation of a-Si:N has been suggested to play an important role in determining the mechanical properties of TiN/a-Si:N nanocomposites [19]. As the overall Si composition varies, the density of the TiN phase within TiN/a-Si:N can be taken as 5.4 g/cm^3 based on the constancy of the TiN lattice parameter. The a-Si:N volume fraction within the TiN/a-Si:N nanocomposites can be calculated as a function of the overall Si composition, assuming that the density of the a-Si:N phase is 3.3 g/cm^3 and does not vary with the overall Si composition. As shown in Figure 9, the calculated a-Si:N volume fraction varies approximately linearly with the overall Si composition, reaching ~ 45% at 20 at. % Si. For three dimensional site percolation, the percolation threshold ranges from 20% to 40% [20]. The Si composition range for the present series of Ti-Si-N coatings thus likely covers the percolation transition region. The crucial question is whether, by manipulating the microstructure of nanocrystalline B1-TiN and a-Si:N on the nm length scale, the mechanical properties of TiN/a-Si:N nanocomposites can be made to significant exceed those of B1-TiN. In the present series of Ti-Si-N coatings, the nanocrystalline TiN grains grow in a columnar-like fashion along the growth direction. With this particular microstructure, the measured elastic modulus and hardness values do not significantly exceed those of B1-TiN. Veprek et al. report that their Ti-Si-N specimens consist of nanocrystalline equiaxed TiN grains [8 11 18]. Whether the microstructural difference between nm scale columnar and nm scale equiaxed TiN grains separated by a-Si:N is responsible for the differences between the mechanical properties reported here and those reported previously by Veprek awaits further clarification.

SUMMARY

In summary, we have performed a detailed examination of the microstructure and mechanical properties of a series of Ti-Si-N coatings with 0 to 20 at. % Si. Structure and atomic short-range order studies show that these Ti-Si-N coatings are TiN/a-Si:N nanocomposites, with nanocrystalline columnar TiN grains. Instrumented nanoindentation measurements show that the coatings are not significantly harder than B1-TiN. Our results highlight the importance of detailed nm-scale microstructural characterization for the understanding of the mechanical response of ceramic nanocomposites.

ACKNOWLEDGEMENT

WJM gratefully acknowledge partial project support from Louisiana Board of Regents through contracts LEQSF(2000-03)-RD-B-03, LEQSF(2001-04)-RD-A-07, and the National Science Foundation through grant #DMI-0124441. The ion beam analysis work at the Argonne National Laboratory was supported by the DOE Office of Science, Basic Energy Sciences, under contract #W-31-109-ENG-38. We thank B. Feng for technical assistance.

Figure Captions

Figure 1. A contact AFM image of the as-deposited surface of a Ti-Si-N coating with a Si composition of 19.2 at. %. The vertical scale on the 4 μm × 4 μm scan is 20 nm.

Figure 2. RBS measurements of the Ti-Si-N composition: (a) RBS spectra of four Ti-Si-N coatings with respectively 0.3, 7.0, 14.2, 19.2 at. % Si, (b) Ti and Si composition of Ti-Si-N coatings as a function of the Si cathode current during deposition.

Figure 3. Cross-sectional TEM image: (a) of a Ti-Si-N/Si(100) specimen with 7.0 at. % Si, (b) of a silicon nitride/Si(100) specimen.

Figure 4. Electron diffraction patterns: (a) cross-sectional SADP of a Ti-Si-N coating with 0.3 at. % Si, (b) cross-sectional SADP of a Ti-Si-N coating with 7.0 at. % Si, (c) cross-sectional SADP of a Ti-Si-N coating with 19.2 at. % Si, (d) plan-view SADP of the same Ti-Si-N coating shown in (c).

Figure 5. X-ray diffraction: (a) a θ-2θ XRD pattern of a Ti-Si-N coating with 19.2 at. % Si, (b) estimated growth direction TiN column height based on Scherrer broadening.

Figure 6. Cross-sectional high-resolution TEM image: (a) of a Ti-Si-N coating with 0.3 at. % Si, (b) of a Ti-Si-N coating with 19.2 at. % Si.

Figure 7. XANES spectra: (a) Ti K-edge spectra from a number of Ti-Si-N coatings and from B1-TiN, the Si composition is noted above each spectrum; (b) Si K-edge spectra from the same set of Ti-Si-N coatings and from a-Si:N; (c) tuned (dot) and 50 % detuned (line) Si K-edge spectra of a Ti-Si-N coating with 7.0 at. % Si.

Figure 8. Instrumented nanoindentation: (a) load vs. displacement curves for a Ti-Si-N coating with 7.0 at. % Si and for the B1-TiN specimen, (b) load vs. displacement curves for a Ti-Si-N coating with 11.9 at. % Si and for the B1-TiN specimen, (c) indentation modulus and hardness of the present series of Ti-Si-N coatings as a function of the Si composition.

Figure 9. Calculated volume fraction of the a-Si:N phase within the Ti-Si-N coatings as a function of the overall Si composition.

REFERENCES:

[1] T. S. Eyre, in Treatise on Materials Science and Technology 13, edited by D. Scott, Academic Press, New York (1979), p. 363.

[2] J. Patscheider, T. Zehnder, M. Diserens, Surf. Coat. Technol. 146/147, 201 (2001).

[3] D. M. Cao, T. Wang, B. Feng, W. J. Meng, K. W. Kelly, Thin Solid Films 398/399, 553 (2001).

[4] S. Veprek, S. Reiprich, L. Shizhi, Appl. Phys. Lett. 66, 1 (1995).

[5] A. A. Voevodin, J. S. Zabinski, Thin Solid Films 370, 223, (2000).

[6] T. Zehnder T, J. Patscheider, Surf. Coat. Technol. 133/134, 138 (2000).

[7] B. Feng, D. M. Cao, W. J. Meng, L. E. Rehn, P. M. Baldo, G. L. Doll, Thin Solid Films 398/399, 210 (2001).

[8] S. Veprek, A. Niederhofer, K. Moto, T. Bolom, H. D. Mannling, P. Nesladek, G. Dollinger, A. Bergmaier, Surf. Coat. Technol. 133/134, 152 (2000).

[9] W. J. Meng, G. L. Eesley, Thin Solid Films 271, 108 (1995).

[10] H. Ljungcrantz, M. Oden, L. Hultman, J. E. Greene, J. E. Sundgren, J. Appl. Phys. 80, 6725 (1996).

[11] S. Veprek, A. S. Argon, Surf. Coat. Technol. 146, 175 (2001).

[12] W. J. Meng, T. J. Curtis, L. E. Rehn, P. M. Baldo, Surf. Coat. Technol. 120/121, 206 (1999).

[13] W. T. Elam, J. P. Kirkland, R. A. Neiser, P. D. Wolf, Phys. Rev. B38, 26 (1988).

[14] F. W. Lytle, R. B. Greegor, D. R. Sandstrom, E. C. Marques, J. Wong, C. L. Spiro, G. P. Huffman, F. E. Huggins, Nucl. Instrum. Methods Phys. Res. 226, 542 (1984).

[15] W. C. Oliver, G. M. Pharr, J. Mater. Res. 7, 1564 (1992).

[16] R.S. Averback, L. J. Thompson, J. Moyle, M. Schalit, J. Appl. Phys. 53, 1342 (1982).

[17] L. E. Toth, Transition Metal Carbides and Nitrides, Academic Press, New York (1971).

[18] S. M. Heald, in X-ray Absorption, Principles, Applications, Techniques of EXAFS, SEXAFS and XANES, edited by D. C. Koningsberger and R. Prins, Wiley, New York (1988).

[19] A. Niederhofer, T. Bolom, P. Nesladek, K. Moto, C. Eggs, D. S. Patil, S. Veprek, Surf. Coat. Technol. 146/147, 183 (2001).

[20] R. Zallen, The Physics of Amorphous Solids, Wiley, New York (1983).

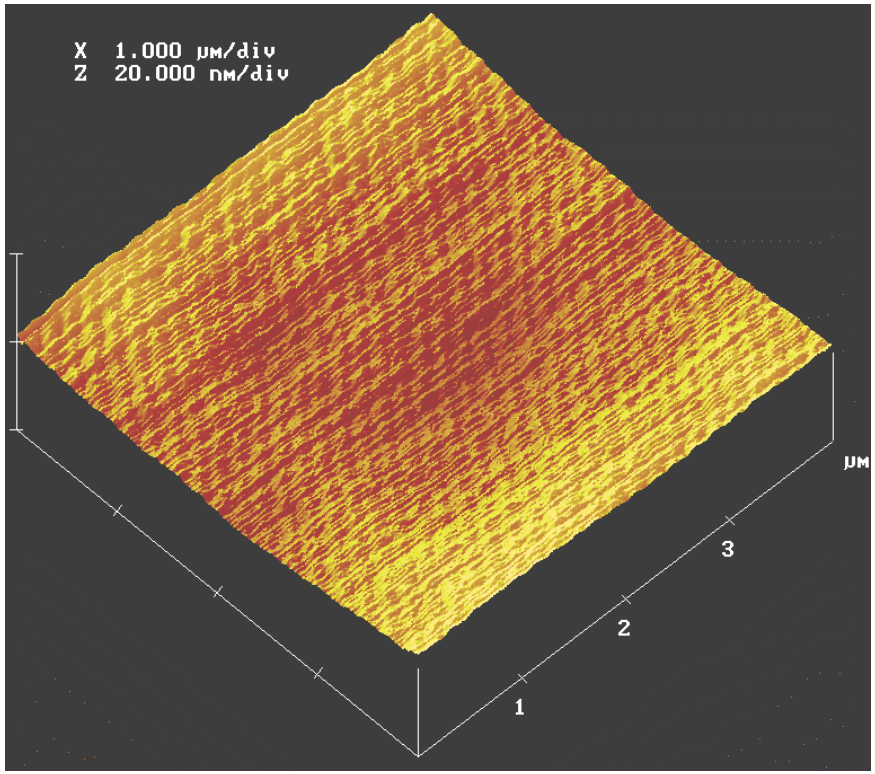

Figure 1

Meng et. al., ICMCTF submission 2002

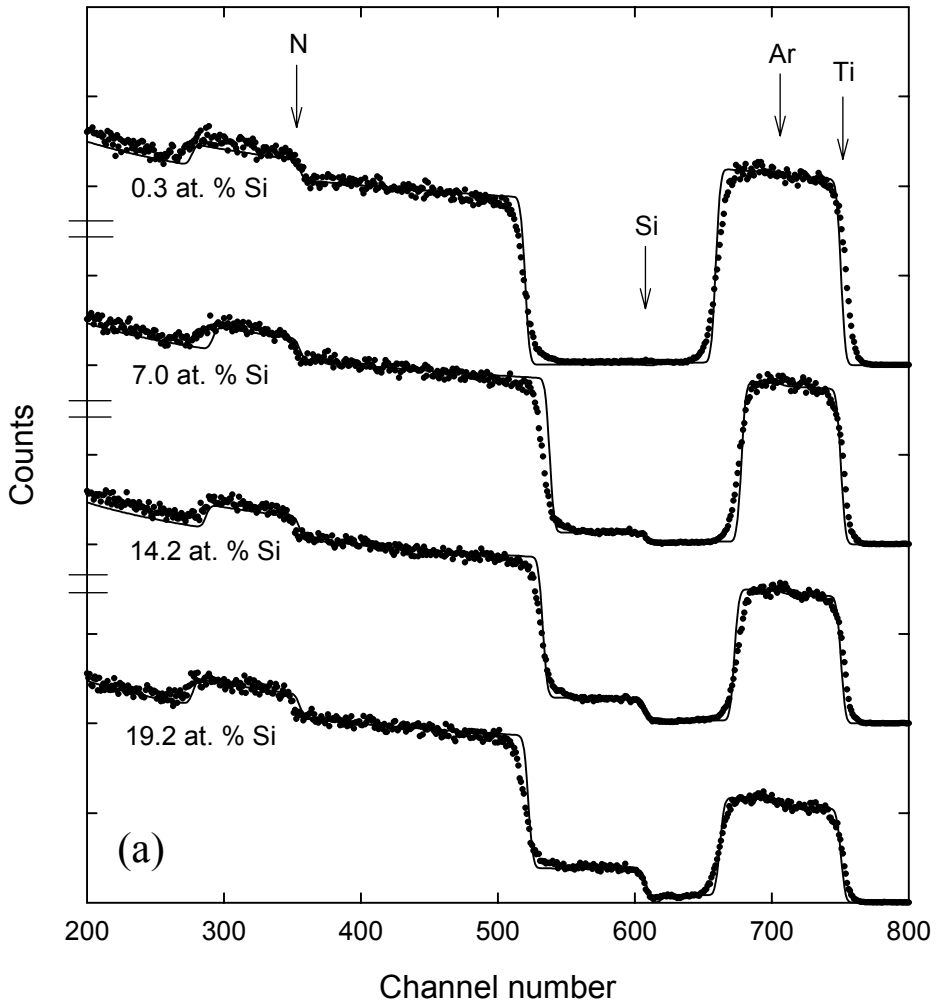

Figure 2

Meng et. al., ICMCTF submission 2002

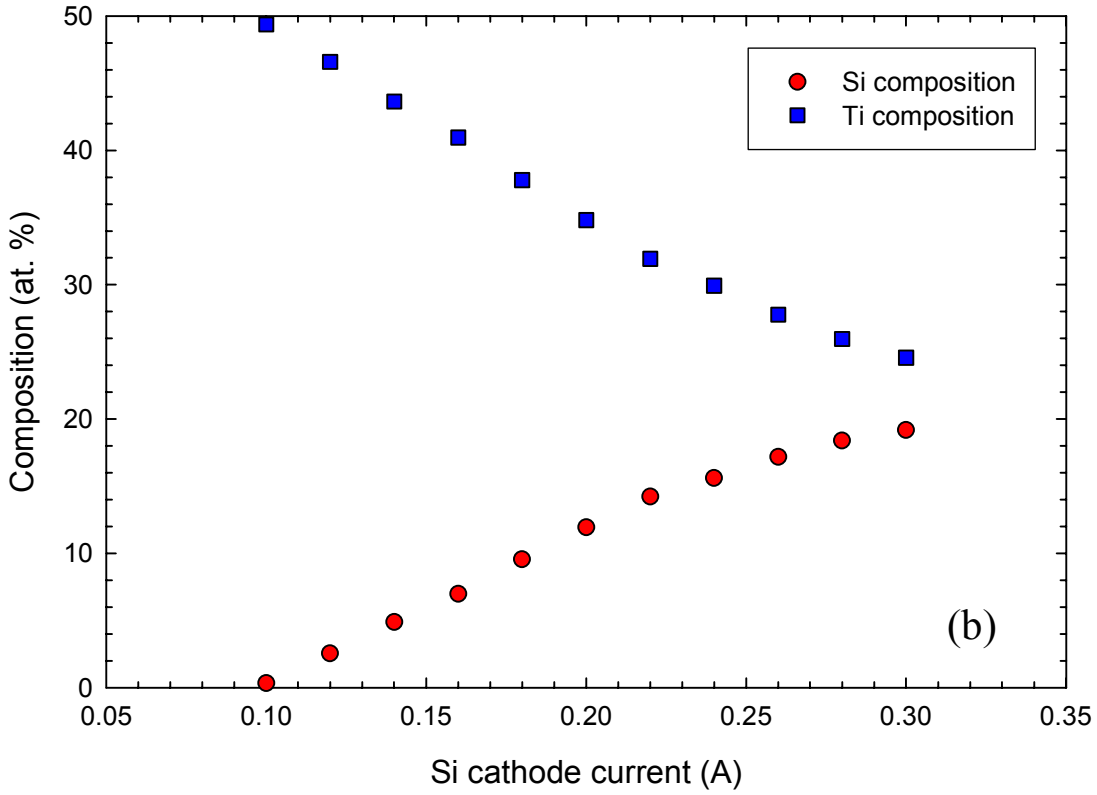

Figure 2

Meng et. al., ICMCTF submission 2002

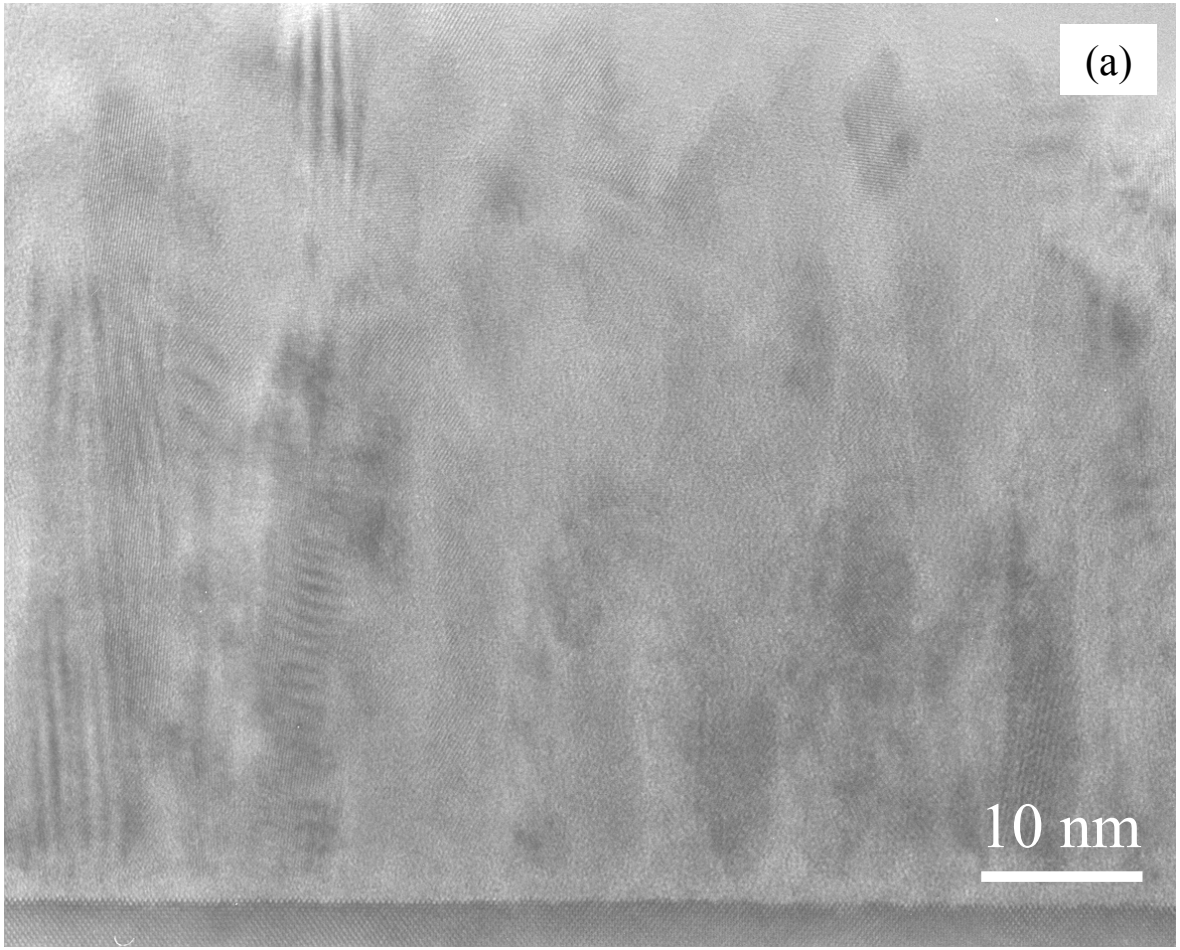

Figure 3 7.0 at. % Si

Meng et. al., ICMCTF submission 2002

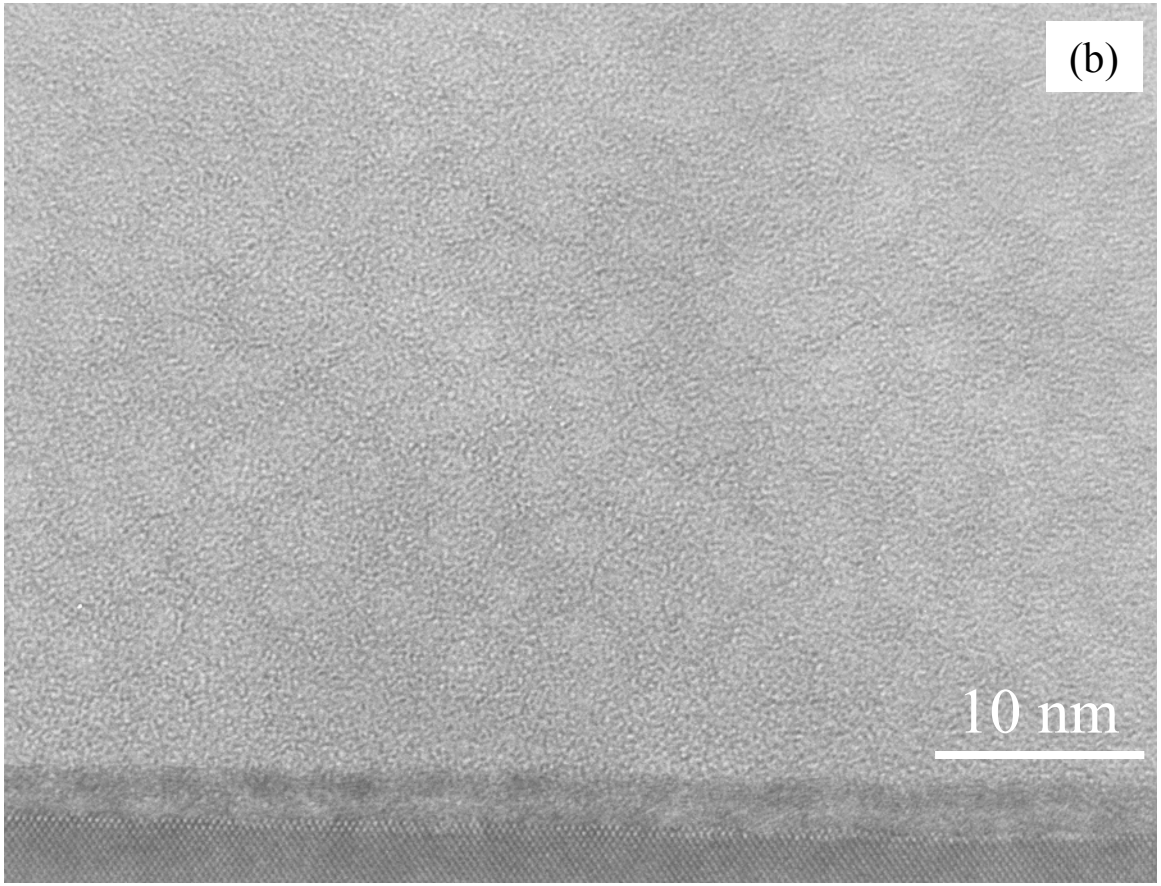

a-Si:N

Figure 3

Meng et. al., ICMCTF submission 2002

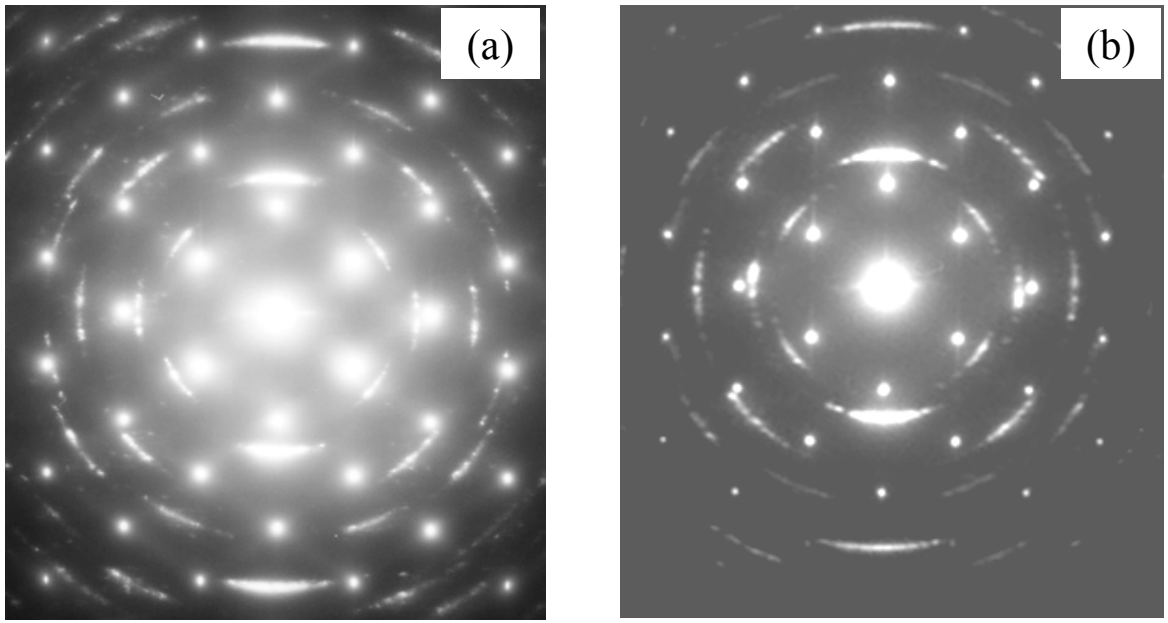

0.3 at. % Si

7.0 at. % Si

Figure 4

Meng et. al., ICMCTF submission 2002

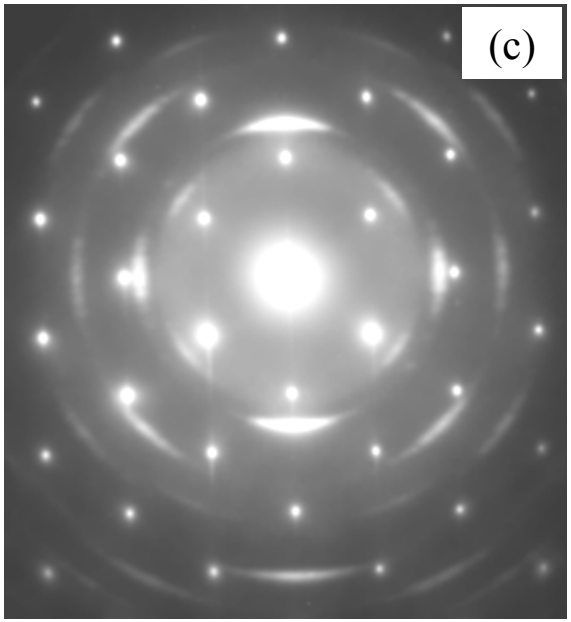

19.2 at. % Si

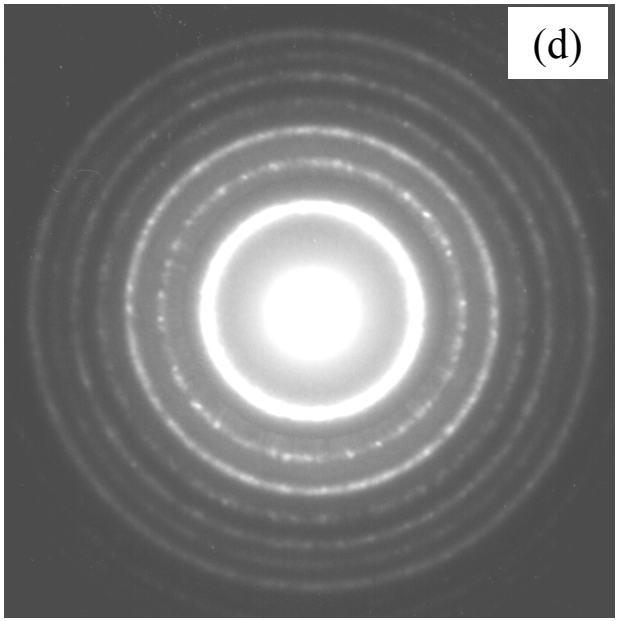

19.2 at. % Si

Figure 4

Meng et. al., ICMCTF submission 2002

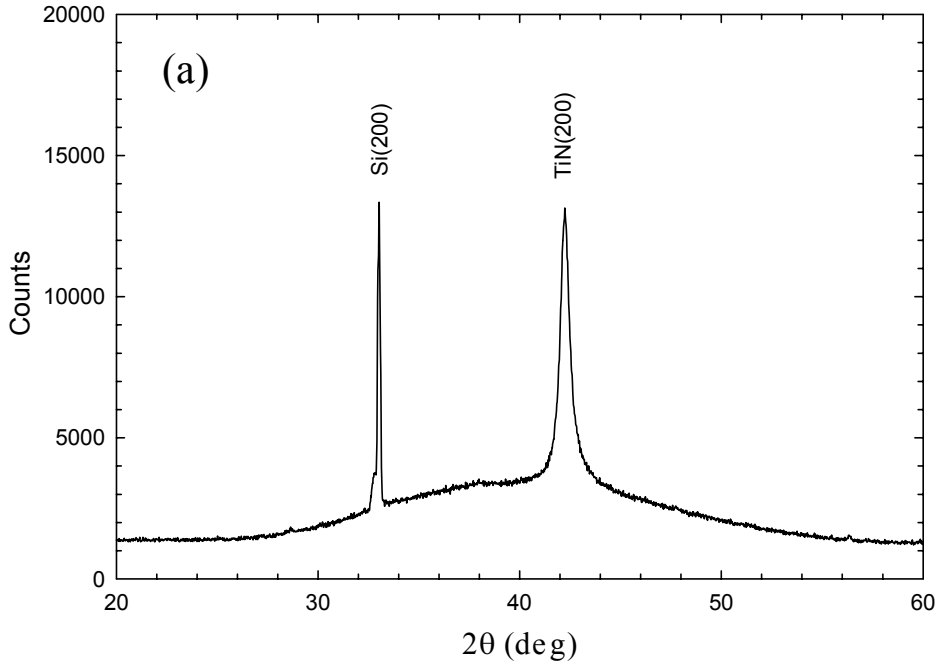

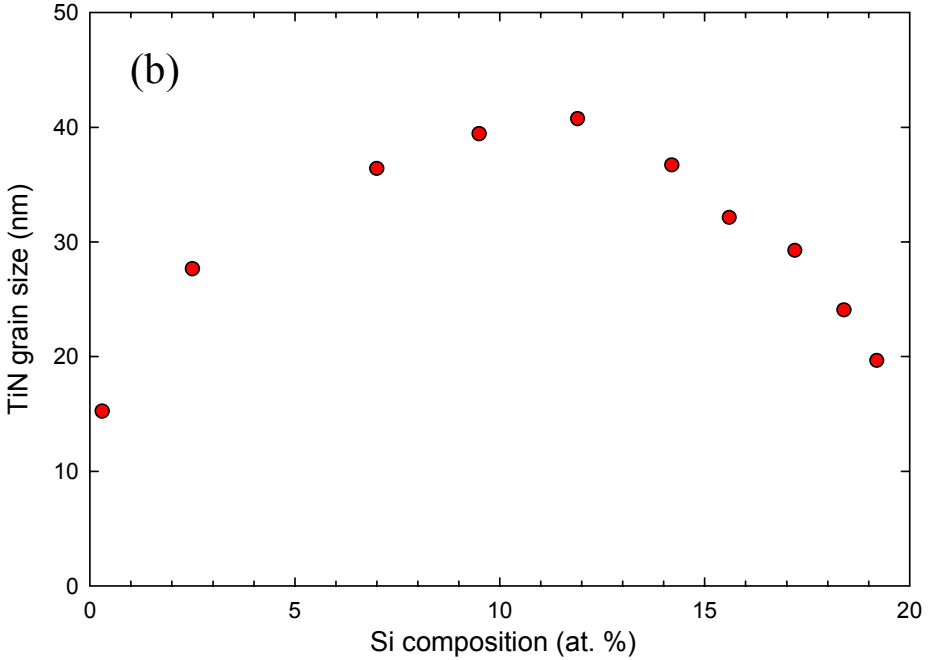

19.2 at. % Si

Figure 5

Meng et. al., ICMCTF submission 2002

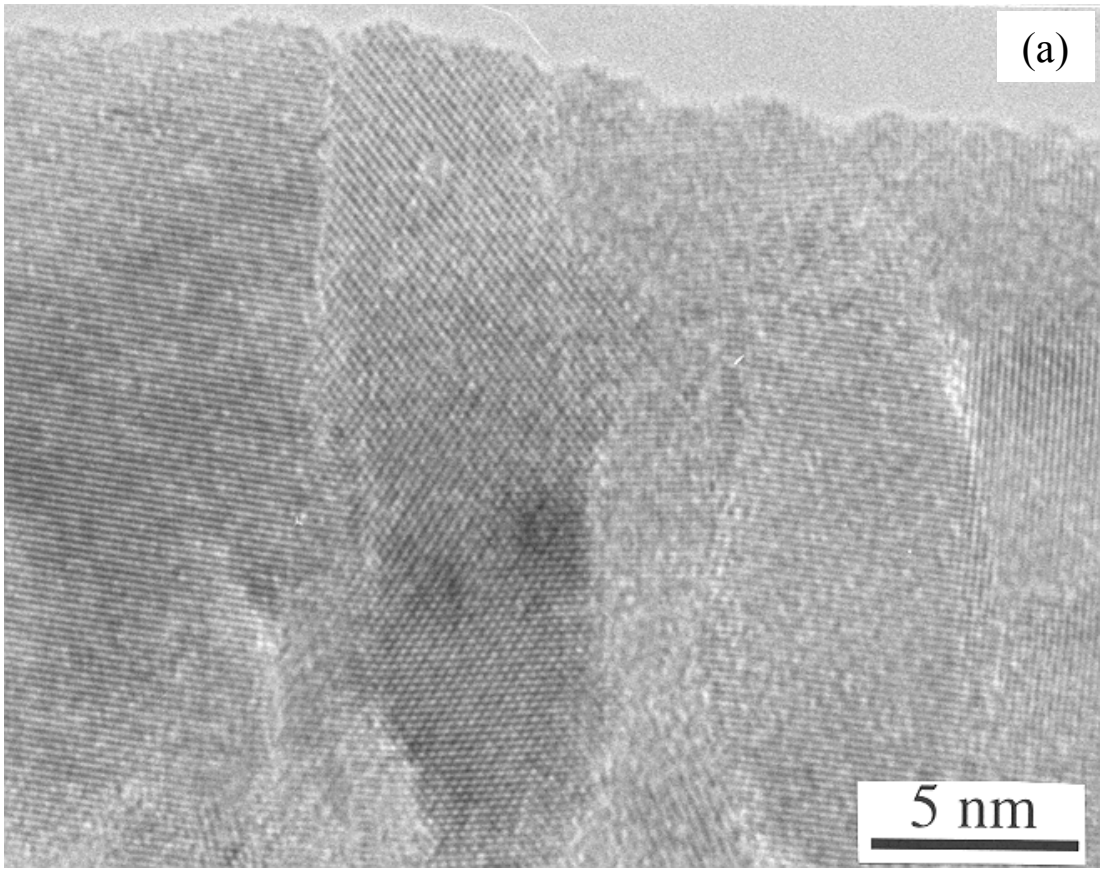

Figure 6

0.3 at. % Si

Meng et. al., ICMCTF submission 2002

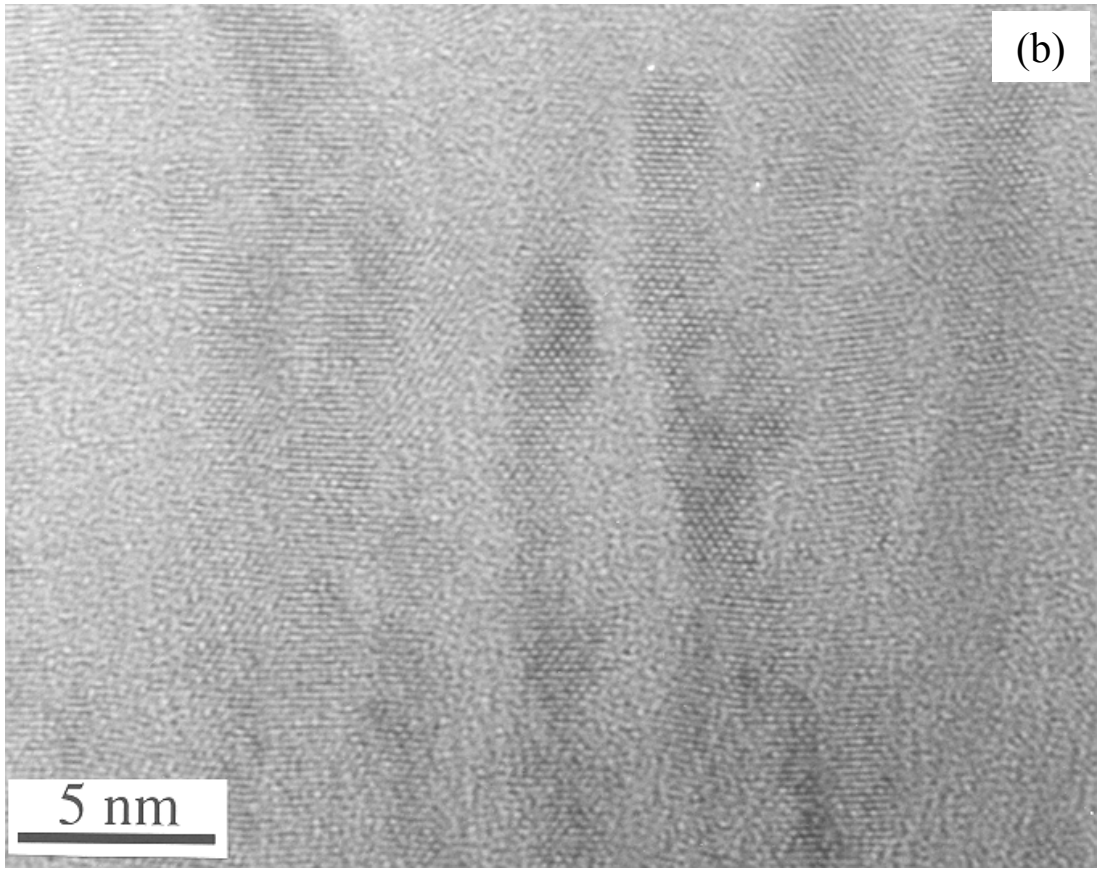

19.2 at. % Si

Figure 6

Meng et. al., ICMCTF submission 2002

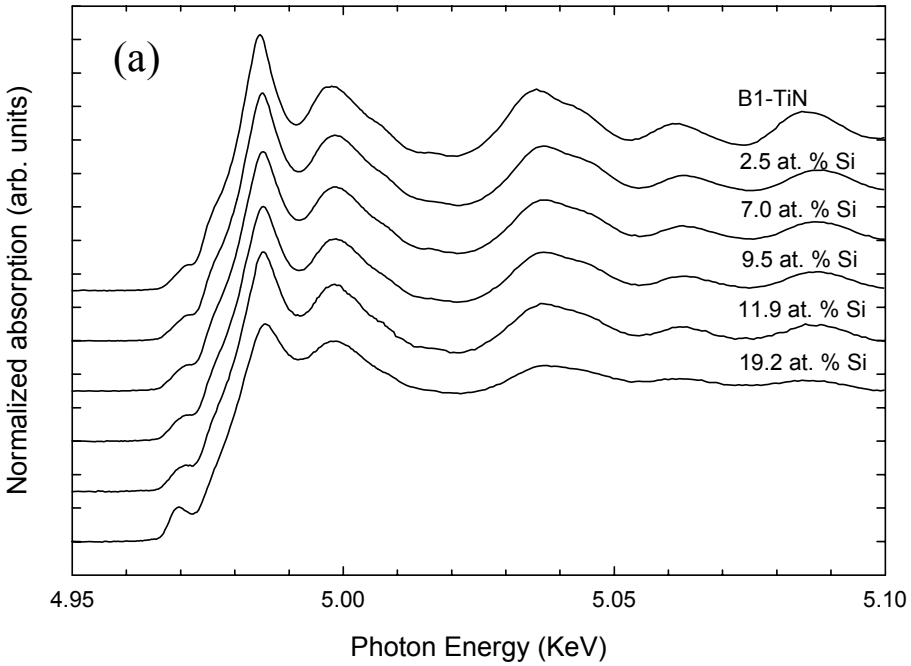

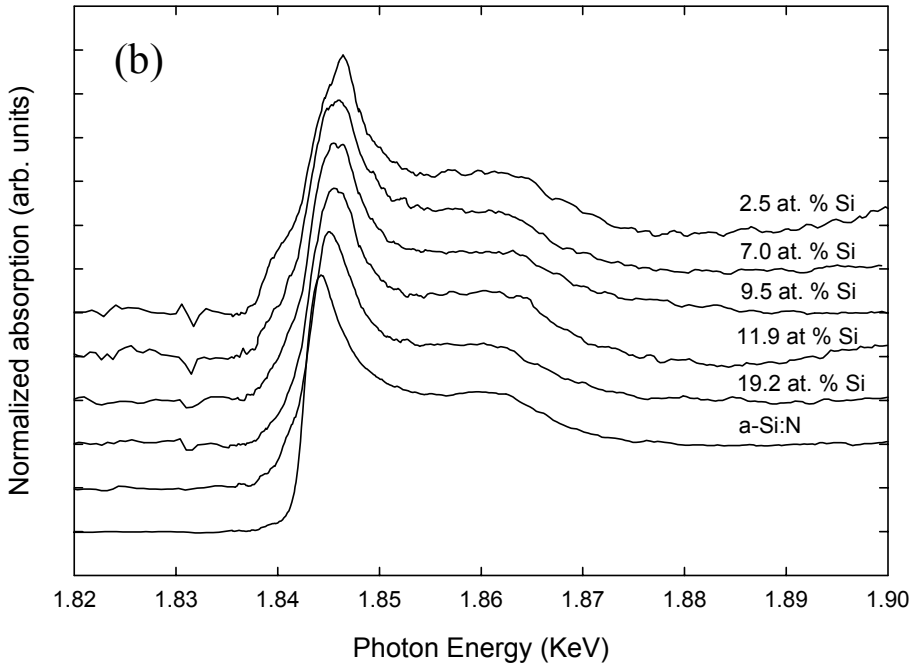

Figure 7

Meng et. al., ICMCTF submission 2002

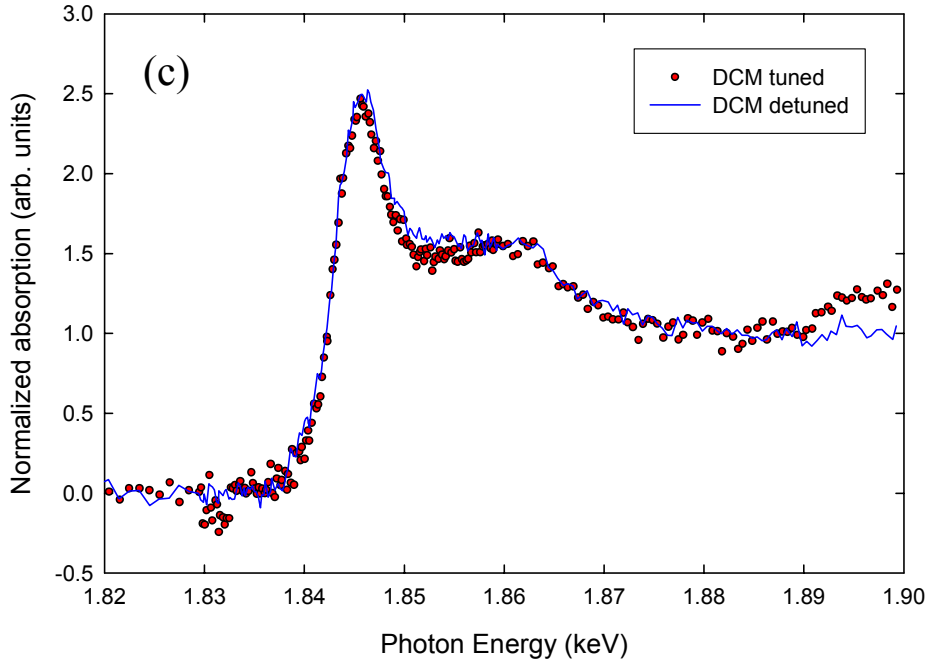

Figure 7

Meng et. al., ICMCTF submission 2002

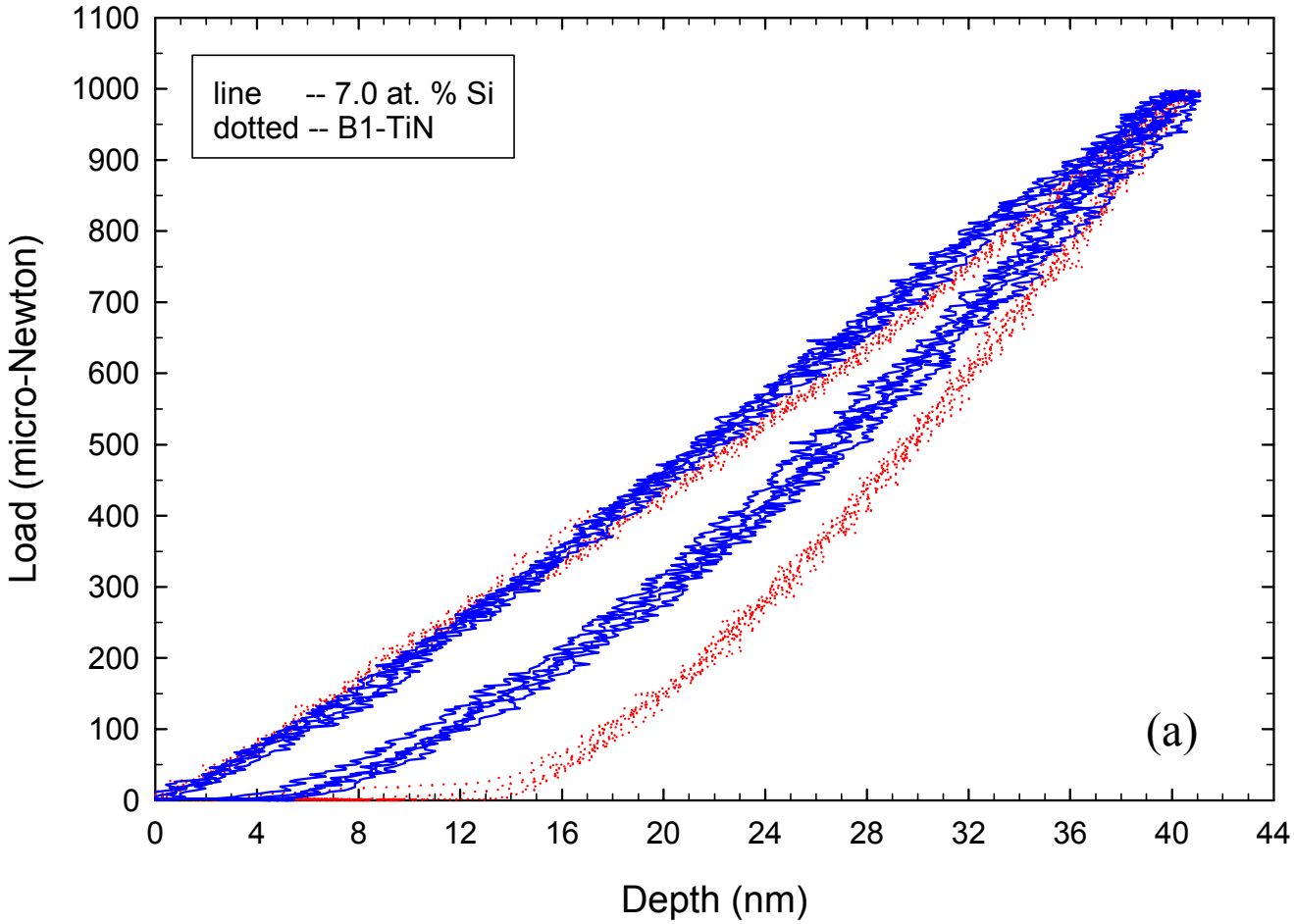

Figure 8

Meng et. al., ICMCTF submission 2002

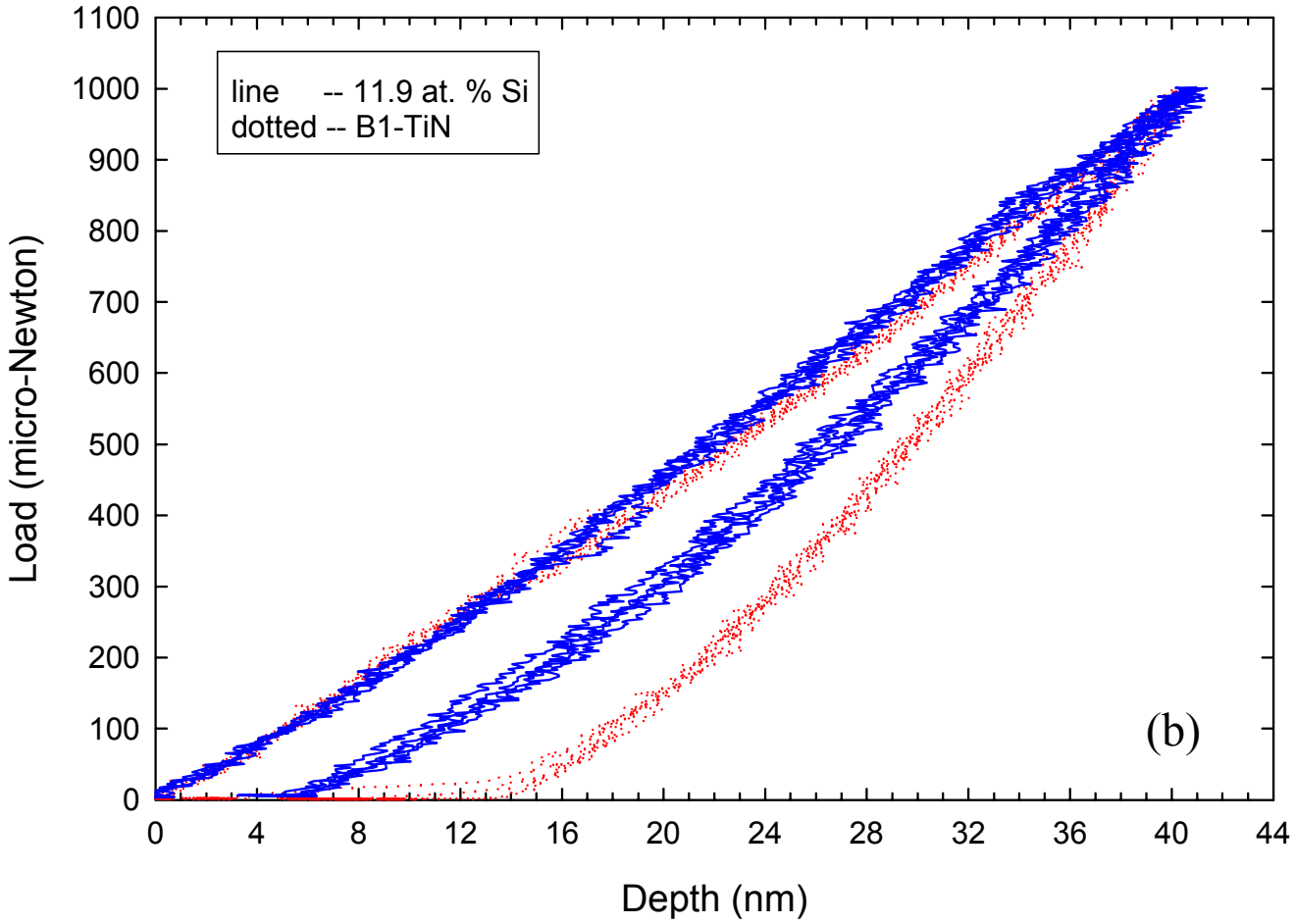

Figure 8

Meng et. al., ICMCTF submission 2002

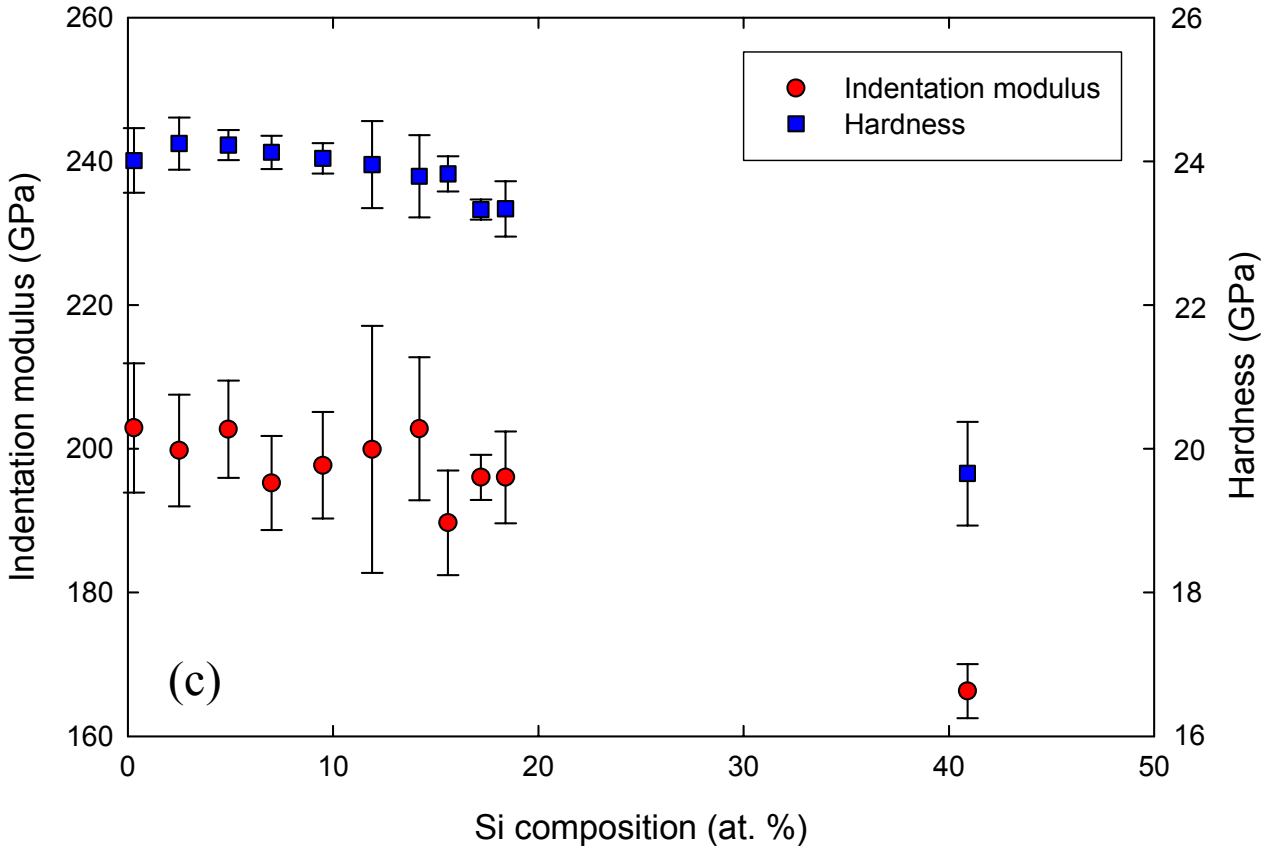

Figure 8

Meng et. al., ICMCTF submission 2002

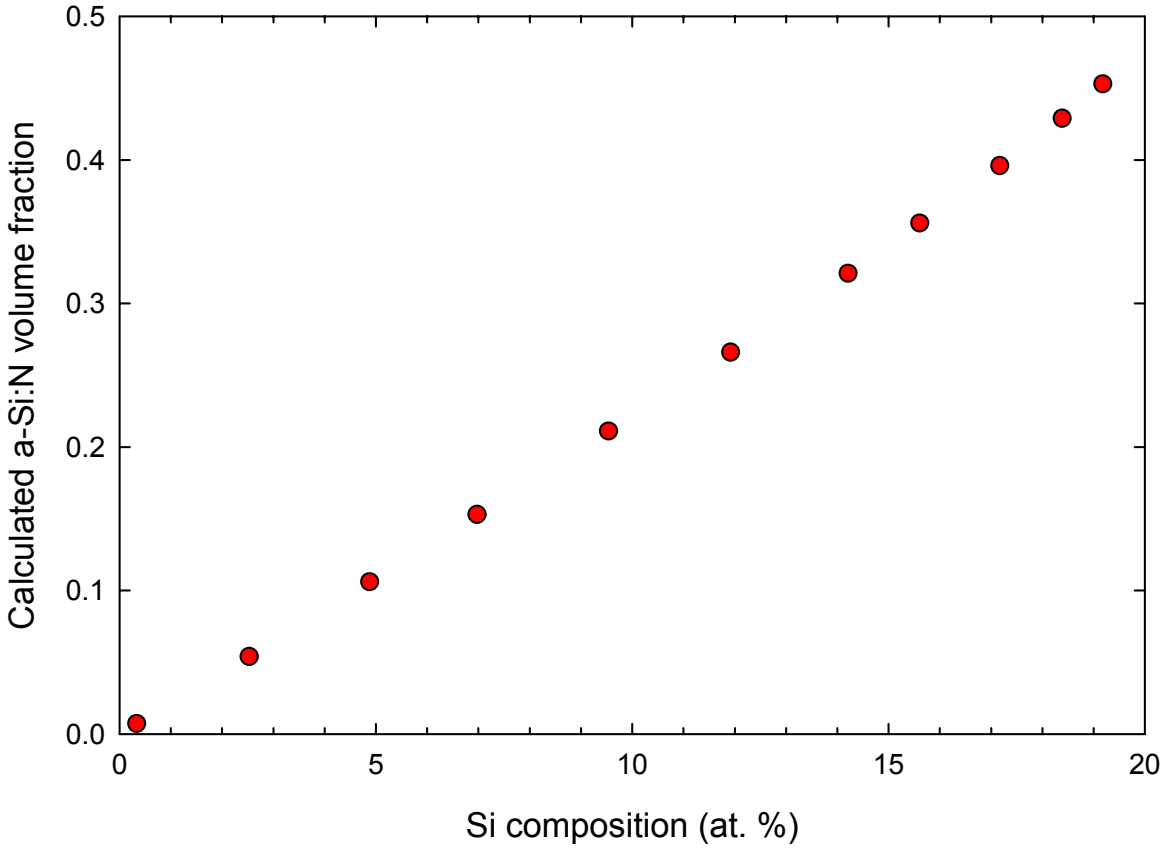

Figure 9

Meng et. al., ICMCTF submission 2002